Modeling distributed kinetics in isolated semiconductor quantum dots

M. Kuno
Naval Research Laboratory, 4555 Overlook Ave. SW, Washington, DC 20375

D. P. Fromm,* S. T. Johnson, A. Gallagher,† and D. J. Nesbitt‡
JILA, National Institute of Standards and Technology and University of Colorado and Department of Chemistry and Biochemistry, University of Colorado, Boulder, Colorado 80309-0440
(Received 29 July 2002; published 14 March 2003)

A detailed modeling of recently observed nonexponential fluorescence intermittency in colloidal semiconductor quantum dots (QDs) is presented. In particular, experiments have shown that both ''on''-time and ''off''-time probability densities generated from single-QD fluorescence trajectories follow an inverse power law, $P(\tau_{on/off}) \propto 1/\tau_{on/off}^{1+\alpha}$, over multiple decades in time, where the exponent $1+\alpha$ can, in general, differ for ''on'' versus ''off'' episodes. Several models are considered and tested against their ability to predict inverse power law behavior in both $P(\tau_{on})$ and $P(\tau_{off})$. A physical picture involving electron tunneling to, and return from, traps located several nanometers away from the QD is found to be consistent with the observed $P(\tau_{off})$ but does not yield the inverse power-law behavior seen in $P(\tau_{on})$. However, a simple phenomenological model based on exponentially distributed and randomly switched on and off decay rates is analyzed in detail and shown to yield an inverse power-law behavior in both $P(\tau_{on})$ and $P(\tau_{off})$. Monte Carlo calculations are used to simulate the resulting blinking behavior, and are subsequently compared with experimental observations. Most relevantly, these comparisons indicate that the experimental on→off blinking kinetics are independent of excitation intensity, in contradiction with previous multiphoton models of on/off intermittency based on an Auger-assisted ionization of the QD by recombination of a second electron-hole pair.

DOI: 10.1103/PhysRevB.67.125304 PACS number(s): 78.55.Et, 78.67.Hc

I. INTRODUCTION

The recent observation of fluorescence intermittency in colloidal semiconductor quantum dots (QDs) is one example of phenomena revealed by observations of photophysics at the single fluorophore level. Since the inception of single molecule spectroscopy in 1989, many such light-induced processes have been seen including the observation of photon bunching/antibunching[1] and spectral wandering,[2] as well as time varying intersystem crossing rates[3] and triplet lifetimes of single molecules.[4] In this respect, single molecule measurements offer the exciting possibility of peeling back the ensemble averaging that obscures these effects, which have thus far been unobservable in traditional ensemble measurements. New opportunities arise for learning about subtle yet fundamental interactions between a single fluorophore and its local molecular environment, which has spawned growing interest in applying single molecule techniques to complex biophysical problems.

''Blinking,'' or fluorescence intermittency, refers to abrupt transitions in the fluorescence ''trajectory'' of a single fluorophore between finite episodes of (i) absorption/laser induced fluorescence, and (ii) periods of darkness where no light is emitted despite continuous laser illumination. This form of emission intermittency has been seen in virtually all systems studied at the single molecule level and includes colloidal semiconductor QDs,[5–14] self assembled QDs,[15] porous silicon,[16] light harvesting complexes,[17] fluorescent proteins,[18–20] single polymer segments,[21] single ions,[22,23] and single dye molecules.[24–26] Apart from universal agreement for the existence of blinking, there appears to be little consensus as to the mechanism or origin behind the effect.

Historically, fluorescence intermittency has been attributed to a number of causes. A natural explanation for blinking is an effect known as quantum jumps, first described by Bohr in 1913 and later by Cook and Kimble in the mid 1980s.[27] Quantum jumps refer to interruptions of a fluorescence cycling transition by infrequent ''jumps'' to a nonemissive metastable shelf state of an ion or atom (or in the case of molecules, a triplet state). This effect has been experimentally verified by a number of groups for single ions confined to radio frequency traps[28] and more recently in single molecules at cryogenic temperatures.[29] In practice, these fluorescence trajectories show discrete jumps between two emission intensity levels, ''on/off,'' and this behavior is often referred to as random telegraph signal (or noise). The qualitative appearance of the trajectories gives direct information about the quantum state of the system. Periods where the molecule is ''on'' refers to episodes of fluorescence cycling between ''bright'' states and periods where the molecule is ''off'' refers to time spent in the nonemissive triplet (or metastable shelf) state.

A direct application of a quantum jump analysis to room temperature studies has not been straightforward. Problems arise because many systems studied to date do not show the single exponential on-time and off-time probability densities $[P(\tau_{on}), P(\tau_{off})]$ expected for a quantum-jump picture.[5–13,20,21,26] Rather, it is often the case that both $P(\tau_{on})$ and $P(\tau_{off})$ exhibit significant nonexponential characteristics, making any quantum jump analysis suspect. To circumvent this problem, other mechanisms have been proposed for explaining the origin of fluorescence intermittency. Some arguments invoke the physical rotation of a molecule's transition dipole relative to the polarization of the incoming exci-

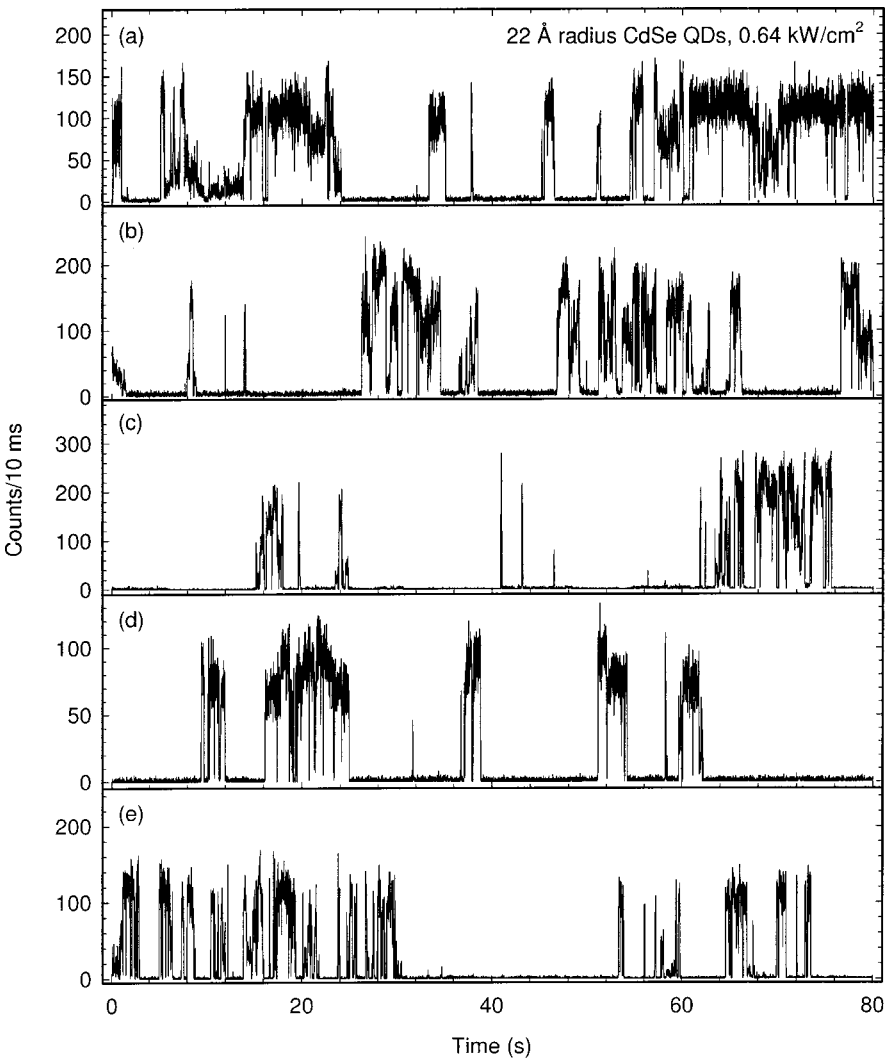

FIG. 1. (a)–(e) Experimental fluorescence trajectories of five isolated 22-Å-radius (ZnS-overcoated) CdSe QDs dispersed onto a fused silica microscope coverslip. Fluorescence intermittency can be seen by brief periods of uninterrupted emission followed by periods of negligible count rates. In all cases, the excitation intensity is 0.64 kW/cm^2, and the integration time of the multichannel scaler is 10 ms. Experimental trajectories typically last 20 min, only a small sample (80 s) of which is shown.

tation, or require dramatic shifts in the molecular absorption in order to account for abrupt ''on'' to ''off'' transitions. Other arguments posit metastable molecular conformations, consisting of local twists in a conjugated molecule's backbone, enhancing nonradiative rates to the ground state thereby accounting for dark periods in the emission.[26] However, many studies have shown no direct correlation between blinking episodes and polarization rotation or spectral shifts in the fluorophore.[30–33] The origin of fluorescence intermittency in isolated systems such as fluorescent proteins and semiconductor quantum dots therefore remains an open and intriguing question.

The fluorescence intermittency observed in colloidal semiconductor QDs is a particularly interesting example of blinking, since long fluorescence trajectories can be followed (frequently $>10^8$ emitted photons) that offer unprecedented statistics on the underlying kinetic phenomena. As an example, previous experiments on ZnS overcoated CdSe QDs have yielded sufficient data to generate event distributions spanning greater than seven decades in probability density and five decades in time.[12] In contrast, many fluorescing objects, such as single molecules and fluorescent proteins, suffer from fast ''photobleaching,'' which typically limits room temperature fluorescence measurements to approximately 10^6 emitted photons. Although the exact mechanism behind photobleaching is not known, it is generally thought to arise from photochemistry that renders the single fluorophore nonfluorescent.[34] The much lower propensity for QDs to photobleach is one reason for keen interest in using these particles in biological fluorescence-tagging applications.[35]

The statistics of fluorescence intermittency in individual semiconductor QDs has recently revealed fascinating kinetics in the on/off blinking phenomenon.[5–14] Of particular interest is that $P(\tau_{on})$ and $P(\tau_{off})$, from fluorescence trajectories of individual InP, CdTe, and CdSe QDs, show an inverse power-law behavior over many decades in probability density and in time.[9–14] This inverse power law is common to *all* QDs we have studied, suggesting a general mechanism behind the on/off fluorescence intermittency, irrespective of the size or composition of the QD. As a key focus of this work, we study possible origins of these distributed kinetics, and other issues related to the blinking phenomenon.

The organization of this paper is as follows. Sample experimental blinking data are briefly presented in Sec. II. A qualitative discussion of various possible mechanisms follows in Sec. III, where the successes and failings of each model are noted in yielding inverse power law kinetics in

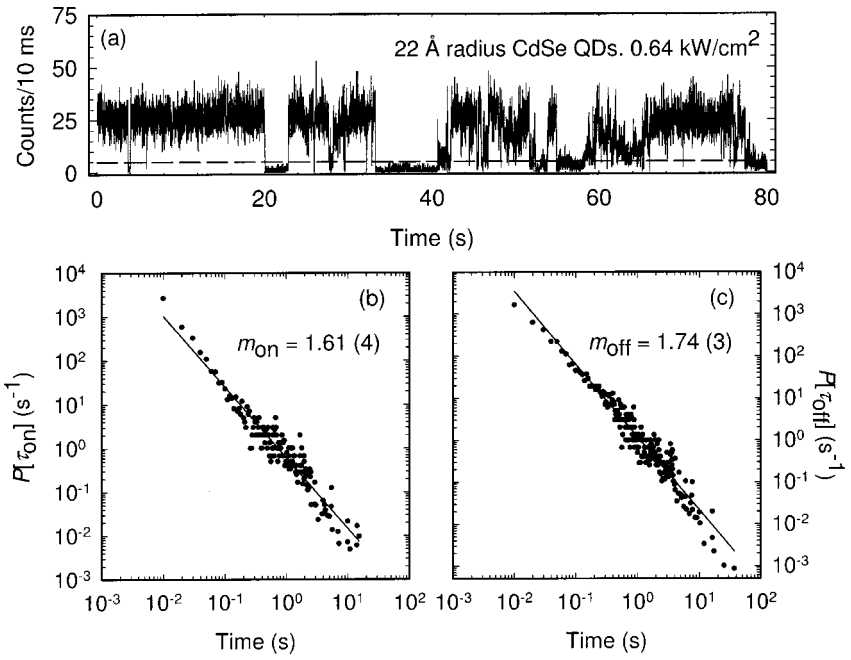

FIG. 2. (a) 80-s segment from the fluorescence trajectory of an isolated 22-Å-radius (ZnS-overcoated) CdSe QD. The dashed line is the intensity threshold defining ''on'' from ''off.'' (b) $P(\tau_{on})$ plotted on a log-log plot. (c) $P(\tau_{off})$ plotted on a log-log plot. In both cases, the line is a linear fit to the data (extracted slopes and errors shown) indicating power law behavior in $P(\tau_{on})$ and $P(\tau_{off})$.

either or both $P(\tau_{on})$ and $P(\tau_{off})$. In Sec. IV a discussion of a phenomenological charging-tunneling model is presented, which in conjunction with Monte Carlo simulations indicates that exponentially distributed and randomly selected on/off decay rates are in best agreement with the data. These predictions are compared with experimental results and used to interpret previously suggested Auger-assisted ionization models for QD blinking. Section V summarizes and concludes the main results.

II. EXPERIMENT

The II-VI CdSe quantum dots used in our experiments are made by the pyrolysis of organometallic precursors in a hot coordinating solvent. The resulting CdSe QDs have sizes tunable between a 10 and 50 Å radius, with surfaces passivated by organic ligands, tri-*n*-octylphosphine oxide (TOPO), and trioctylphosphine. The CdSe QDs are subsequently overcoated with a few monolayers of ZnS to passivate surface sites that suppress the luminescence. Further details about the QDs and their characterization can be found in Refs. 36–40. Fluorescence measurements are performed with a confocal microscope where QDs are illuminated with the 488-nm line of an Ar^+ laser, using a typical focal spot size of $\approx$300 nm and an intensity of $\approx$0.1–100 kW/cm^2. The resulting fluorescence is imaged onto an avalanche photodiode (APD), with ''trajectories'' (i.e., fluorescence count rates versus time) obtained with a commercial multichannel scaler. Details can be found in Refs. 11–13.

To clarify the nature of the fluorescence intermittency, Fig. 1 shows several intervals ($\approx$ 80 s each) randomly selected from the fluorescence trajectories of five different 22-Å radius, ZnS-overcoated, CdSe QDs on a flame-cleaned, fused silica microscope coverslip. In all cases, the QDs are continuously illuminated at an intensity of $I_L = 0.64$ kW/cm^2. Fluorescence intermittency is clearly evidenced by discrete ''on'' episodes of bright fluorescence alternating with ''off'' periods of negligible emission, as first reported for colloidal CdSe QDs by Nirmal *et al.*[5] in 1996. The collected fluorescence trajectories generally span 20 min, although some have exceeded two hours ($>10^9$ absorbed photons and $>10^8$ emitted photons for these excitation intensities), showing the robustness of the QDs against photobleaching.

Analysis of the fluorescence intermittency begins by defining an intensity threshold above or below which the fluorescence is considered ''on'' or ''off,'' [11–13] typically chosen to be $(2–3)\sigma$ greater than background APD noise levels. The dashed line in Fig. 2(a) illustrates the procedure for a sample fluorescence trajectory. Histograms of number of events versus τ_{on} and τ_{off} binned in integral units of a minimum time interval (τ_{min}), are generated with this criterion and weighted by the local density of events to generate the on/off probability densities $P(\tau_{on})$ and $P(\tau_{off})$. Figures 2(b) and 2(c) are log-log plots of $P(\tau_{on})$ and $P(\tau_{off})$ for the CdSe QD shown in Fig. 2(a), using a bin time $\tau_{min}=10$ ms; note that both $P(\tau_{on})$ and $P(\tau_{off})$ exhibit a linear log-log relationship characteristic of an inverse power law with an exponent (i.e., slope) of m_{on} or m_{off}. An explicit demonstration of this power-law behavior down to even shorter times (200 μs/bin) was shown in Ref. 12 for both on and off distributions.

Fluorescence trajectories truncated to encompass only 100, 1000, and 10000 off events out of the full ensemble also yield the same inverse-power-law behavior and slope within experimental uncertainty.[12] This indicates that gradual changes in the QD or its local environment, for example causing some elementary rate process to slowly change over many switching episodes, are not responsible for the observed power-law behavior. Indeed, we observe no correlation between the duration of a given ''on'' (''off'') episode and the next on/off episodes,[12,13] which implies an absence of memory even for adjacent events. Finally, we have found neither a temperature nor laser intensity dependence to the

slopes ($m_{on/off}$) of $P(\tau_{on})$ and $P(\tau_{off})$ for ZnS-overcoated CdSe QDs, tested by varying temperatures and intensities between 300 and 400 K and 0.1 and 100 kW/cm^2, respectively.[12] Other experiments have established this $m_{on/off}$ temperature insensitivity over the much larger range from 300 down to 10 K, unambiguously verifying that on or off switching events are not thermally activated.[9] The analysis presented herein represents an attempt to formulate a physical picture consistent with all these observations, and thereby further elucidate the fluorescence intermittency of isolated semiconductor QDs.

III. PHYSICAL MODELS FOR QD BLINKING

A. Background

It is commonly suggested that blinking or fluorescence intermittency in semiconductor QDs arises from low probability photoionization events that eject a carrier from the particle.[5–13,41] This carrier is presumably an electron rather than a hole due to its smaller effective mass. The QD that is left behind is positively charged and nonfluorescent due to efficient quenching of subsequent electron-hole pairs by the unpaired carrier.[41] Why this additional carrier is not immediately ejected after absorbing the energy from subsequent electron-hole pair recombinations is not established, although a large barrier to hole escape may be responsible. Recovery of the fluorescence occurs when the ejected carrier returns to the nanoparticle through either a thermally activated or barrier tunneling event. Preliminary charge blinking studies of (ZnS-overcoated) CdSe QDs support this hypothesis, showing evidence that the nanoparticles become positively charged under continuous laser excitation.[42] In this manner one can qualitatively rationalize on/off episodes of isolated QDs as arising from ionization and subsequent neutralization events. Other plausible causes, such as the appearance and disappearance of (highly nonradiative) QD surface traps due to atomic or chemical changes, do not alter the basic complications inherent in explanations of nonexponential on/off switching behavior. Thus, in the interest of simplicity, we cast our discussion in the context of a charging model as the most probable cause of on/off QD switching.

The major challenge for a model of fluorescence intermittency is to rationalize *how* the carrier is (i) ejected from a QD and (ii) induced to return to it. Furthermore, the origin of the extremely broad range of switching times needs to be explained. In what follows, we discuss various ways through which an electron can leave and return to the QD. Principal mechanisms include classically allowed ''over the barrier'' processes such as a thermal/Auger-assisted ionization from the lowest excited state[5,8] by recombination of a second electron-hole pair. Alternatively, barrier tunneling events can provide a path by which the carrier leaves the particle.[9,11–13] The importance of quantum tunneling is evident from the observed redshift of the QD band edge absorption upon overcoating, indicating extensive delocalization of carrier wave functions into the outer semiconductor cladding.[36–38]

Figure 3 shows a band-energy diagram for a 27-Å radius (ZnS-overcoated) CdSe QD on a FS surface, with electron and hole traps present in the surrounding substrate. As illustrated, a relatively large >3-eV barrier is expected between the conduction bands of CdSe ($E_{C\,QD}$) and the substrate ($E_{C\,FS}$), which immediately impacts the role of direct thermal ionization versus either direct (Fig. 3, process No. 2) or Auger-assisted tunneling (Fig. 3, process No. 1). Specifically, the rates of thermally activated processes would be governed by $\gamma_{thermal} \approx A \exp(-\Delta E/kT)$, where ΔE is the barrier height and A the pre-exponential electron attempt frequency. For a simple one-dimensional tunneling model, on the other hand, $\gamma_{tunnel}(\Delta E) = A \exp(-\sqrt{8m\Delta E/\hbar^2}\,l)$, where the exponent takes on the numerical value of $\sqrt{\Delta E(eV)}\,l(\text{Å})/1$ Å for a free-electron mass, barrier width (l, in Å) and barrier height (ΔE, in eV). Note that in three-dimensional tunneling from r_1 to r_2, the exact tunneling expression $\gamma_{tunnel}(\Delta E)$ for a constant barrier is essentially equivalent to replacing the l of one-dimensional tunneling with Δr. In addition, there are slowly varying prefactors, which contribute negligibly to the r dependence and can be ignored in a first approximation. This square root versus linear tunneling exponent dependence on ΔE has important consequences; specifically, for barrier heights of order 1 eV and comparable preexponential

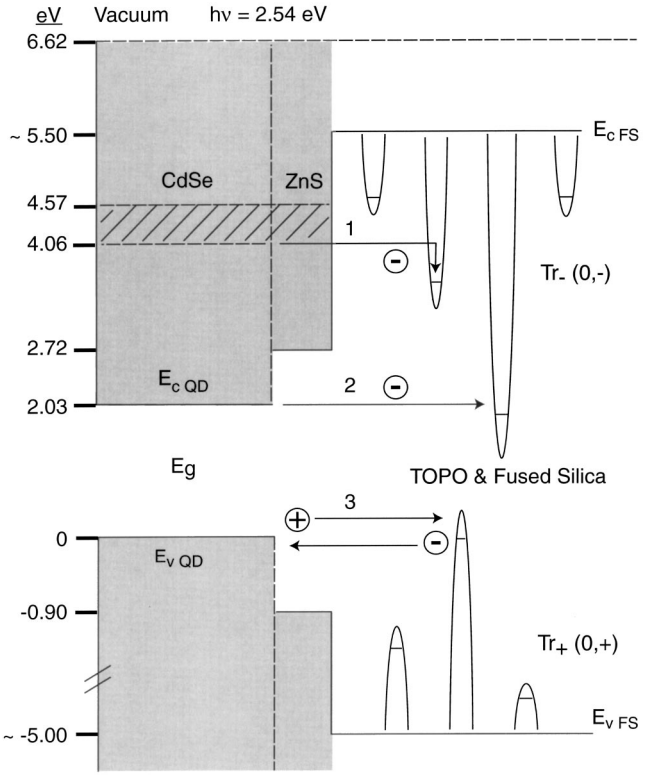

FIG. 3. Band energy diagram of a positively charged 27-Å-radius (ZnS-overcoated) CdSe QD. Relevant positive ion (neutral or positively charged) or negative ion (neutral or negatively charged) ''trap'' sites in or on the fused silica are denoted by Tr_+ and Tr_- respectively. Energies are assigned relative to the top of the CdSe valence band ($E_{vb\,QD}$). Possible electron/hole transitions are depicted by the numbered arrows. Process No. 1: Auger-assisted electron ejection. Process No. 2: Direct electron tunneling to a trap state. Process No. 3: Hole ejection or alternatively, electron injection into the valence band.

A factors, tunneling will dominate over room temperature thermal processes for traps up to ≈5 nm from the QD. This is consistent with the experimentally confirmed lack of temperature dependence by the blinking kinetics. Based on a tunneling model, therefore, the experimentally observed timescales for blinking must arise from a relatively narrow range of trap distances. For example, for a typical prefactor of $A \sim 10^{14}/s$; a free-electron mass in the fused silica and barrier heights with respect to vacuum of ≈4 eV, the fastest ($\approx 10^4$/s) and slowest ($\approx 10^{-2}$/s) blinking rates would correspond to tunneling distances ≈1 and ≈2 nm away from the QD. This dramatically underscores two points: (1) a *small* range of tunneling distance can map into a large dynamic range of kinetic time scales for blinking, and (2) the charging dynamics necessarily involve sampling regions *exterior* to the QD.

A commonly invoked model for QD charging is based on double electron-hole pair formation, followed by single pair recombination and QD ionization via an ''Auger-assisted'' tunneling of either the remaining electron or hole. If we consider the energy dependence of this process, the rate of Auger ionization per conduction band electron would be proportional to $g^* \gamma_{\text{tunnel}}(\Delta E_C - E_g)$, where g^* is the photostationary fractional population in the excited state, $\Delta E_C = E_{C\,\text{FS}} - E_{C\,\text{QD}}$ is the tunneling barrier, and E_g is the CdSe QD band-gap energy provided by carrier recombination. Hole tunneling, i.e., electron transfer from the fused silica to the QD (process No. 3 in Fig. 3) is also possible and will be discussed below. The maximum available energy for Auger-assisted photoejection via one photon plus a second electron-hole pair recombination is $E_g + h\nu \approx 4.57$ eV, with as little as 2 E_g(≈4.06 eV) if relaxation to $E_{C\,\text{QD}}$ takes place prior to the Auger event. If this exceeds the conduction band barrier (ΔE_C), direct Auger ionization of a conduction-band electron can occur at a rate $g^* \gamma_{\text{exc}}$ where γ_{exc} is the rate of laser excited electron-hole generation. Since γ_{exc} and g^* are typically $>10^6$/s and $>10^{-2}$, respectively, the QD will rapidly ionize, becoming dark according to the charging model. Indeed, little or no QD fluorescence is observed on conventional (borosilicate glass) cover slips, which is attributed to a sufficiently small ΔE_C to allow direct ''over-the-barrier'' ionization. Conversely, the fact that little or no QD charging occurs on fused silica cover slips at low light intensities,[42] thus permitting strong QD fluorescence to be observed for long periods, implies ΔE_C to be larger than ≈4.57 eV. This observation rules out any direct Auger charge ejection over the barrier, though Auger-assisted carrier *tunneling* would still be feasible.

Since comparable reverse barrier heights exist for electron return to the QD, this process must also be dominated by tunneling. A photon-assisted QD neutralization is unlikely, as it has generally been observed that the off-time distribution is essentially independent of laser intensity.[5,8,9,11–13] From Fig. 3 it is evident that trap depths relative to the barrier ($E_{C\,\text{FS}}$) must be >1.5 eV to energetically allow electron tunneling from the QD. Likewise, to obtain the necessary dynamic range of electron-return rates requires vacuum tunneling distances $l \sim 1-2$ nm, as described earlier, with negligible contributions from lower barrier tunneling through the ZnS cladding and the TOPO ligands. One central conclusion is that both the on→off and off→on switching times thus require traps extrinsic to the QD, essentially in or on the surface of the fused silica substrate.

In principle, transient heating due to the absorption of incident 488-nm photons could influence the distribution of ''on''/''off'' rates. However, based on the bulk CdSe heat capacity[43] ($C_P \sim 52$ J/mol °C), the temperature of a 27-Å radius QD (mass $\sim 5 \times 10^{-19}$ g) will only experience a ~2 K increase for the complete nonradiative relaxation of a 488-nm photon. Furthermore, using the bulk conductivity [$k_{\text{Fused Silica}} \sim 0.0138$ J/s cm °C (Ref. 43)], this heat dissipates to the underlying fused silica substrate on a timescale of ~10 picoseconds. This is four orders of magnitude faster than the average time between absorption events (≈100 ns) for typical excitation intensities ($I_L \sim 1$ kW/cm^2) and experimentally measured QD absorption cross sections [$\sigma_{488} \sim 4 \times 10^{-15}$ cm^2 (Ref. 12)]. It is therefore reasonable to assume that thermal variations due to the absorption of incident photons are not responsible for an ''on''/''off'' inverse-power-law behavior. Similar conclusions regarding the absence of substantive heating effects have been obtained in spectral diffusion studies of single semiconductor QDs.[44]

To summarize relevant conclusions, the observed range of ''on'' to ''off'' blinking timescales ($10^{-4}-10^2$ s) necessarily involves trap states *external* to the QD. This should be contrasted with *surface* traps on the QD, where much faster tunneling rates can compete more effectively with the $10^{-7}-10^{-8}$ s fluorescence lifetime and thereby influence emission quantum yields. While tunneling of conduction-band electrons to external trap sites is the only significant pathway available at low light intensities (e.g., process No. 2), an Auger-assisted tunneling process (e.g., process No. 1) could in principle also play an important role at the >0.1-kW/cm^2 intensities more typical of single-QD experiments.

B. Activated Arrhenius model

Given possible ionization pathways and likely sites to which the electron localizes, we consider several models. One can immediately reject a quantum jump picture, which, as described earlier, refers to random interruptions of a fluorescence cycling transition by infrequent jumps to a single, nonemissive ''dark'' state.[27–29] As noted previously, this predicts exponential probability densities for both $P(\tau_{\text{on}})$ and $P(\tau_{\text{off}})$, i.e., qualitatively inconsistent with what is observed for isolated semiconductor QDs. Furthermore, the long timescale of the intermittency would be inconsistent with calculated lifetimes of such nonemissive QD electronic states.[41]

The mechanism that at first most simply rationalizes the distributed kinetics in $P(\tau_{\text{on}})$ and $P(\tau_{\text{off}})$ is an Arrhenius model. Historical precedence for this approach lies in the model of Randall and Wilkins,[45] developed to explain inverse power-law behavior in the phosphorescence decay of amorphous semiconductors. This model assumes the existence of (i) an exponentially distributed density of trap states versus trap depth (E_T), i.e., $\rho(E_T) \propto \exp(-\alpha E_T)$; (ii) an exponential dependence of trap-phosphorescence decay rates

versus depth, i.e., $\gamma(E_T) \propto \exp(-E_T/kT)$; and (iii) a distribution of photoexcited carriers ''trapped'' within the material. These assumptions lead analytically to an $I(\tau) \propto \tau^{-m}$ phosphorescence decay with $m = 1 + \alpha kT$, where $1/\alpha$ reflects the $1/e$ depth of the exponential trap distribution. It is important to recognize that this power law behavior results from a static ensemble of trapped carriers, each decaying exponentially in time. Thus, when applied to a single QD with many static trap states, this correctly predicts an inverse power law off→on recovery. However, the rate for electron ejection to such an ensemble of static trap states would go as the *sum* over all individual transitions, thus incorrectly predicting exponential kinetics for on→off blinking. An additional problem with the QD Arrhenius model is the lack of any observed temperature dependence; temperature measurements from 300–400 K show no changes in m for on→off or off→on switching, whereas the predicted $m = 1 + \alpha kT$ behavior yields variation significantly greater than experimental uncertainty.[11–13] More conclusively, cryogenic studies conducted over a much larger dynamic range between 10 and 300 K also reveal m to be temperature insensitive, effectively ruling out any thermally activated mechanism.[9]

C. Charging-tunneling model

Following previous suggestions,[41] we assume that a neutral QD fluoresces and a charged QD is dark. An electron tunnels out of the QD through an external barrier to a trap a distance l from the QD surface. Auger assisted ionization via tunneling (process No. 1, Fig. 3) may dominate QD charging at typical I_L values used in single QD fluorescence experiments; however, the following model applies equally well to tunneling electron loss from the conduction band (process No. 2, Fig. 3) by simply making the tunneling prefactor independent of I_L. Replacing electron loss/return with hole loss/return, i.e., electron transfer to and from neutral/positive trap states (process No. 3, Fig. 3), yields equivalent results in the following model, but for simplicity we assume only conduction band electron transfer to and return from trap states that are either neutral or negatively charged (process No. 2). We also assume that electrons leave and return to the QD by tunneling to relatively deep traps in the fused silica bandgap with attachment energies >1.5 eV for which FS surface states or impurities are probably responsible. Cooling rates are on the order of $\sim 10^{12}$/s, so that tunneling escape based on energy pooling from two pair electron-hole annihilation events can be limited to ≈ 1 ps. Note that in the absence of phonon assisted tunneling (ruled out by temperature independence), the trap state must be deep enough to place it below 4.06 eV in Fig. 3.

We now consider a neutral (fluorescing) QD surrounded by an array of trap sites on the FS surface that are energetically accessible to tunneling at Auger levels of excitation (≈ 4.06 eV). The average QD charge, Q, will follow a rate equation

$$\frac{dQ}{d\tau} = -\sum_i \gamma(l_i) Q, \tag{1a}$$

where

$$\gamma(l_i) = A \exp(-l_i/l_0) \tag{1b}$$

is the tunneling rate to site i, $l_0 = 1$ Å $(1\ \text{eV}/\Delta E)^{1/2}$ is the characteristic electron tunneling distance from the QD to the trap through an average barrier ΔE, and $A \sim 10^{14}$/s is a typical electron escape attempt frequency. Replacing the trap subscript (i) with its location l and assuming a distribution, $\rho(l)$, of trap sites, Eq. (1) yields

$$Q(\tau)/Q_0 = \exp(-\tau/\tau_0), \tag{2a}$$

where

$$\tau_o^{-1} = \sum_i \gamma(l_i) = \int \rho(l)\gamma(l)dl. \tag{2b}$$

Furthermore, the fractional probability that an ionization event fills a trap at distance l is

$$f(l) = \rho(l)\gamma(l) / \int \rho(l)\gamma(l)dl. \tag{3}$$

yielding an *exponentially* decaying distribution of distances to neighboring trap sites.

We next consider the electron recovery process. If the carrier can only return to the QD from the initially filled trap (i.e., no trap-to-trap transfer), the average time dependence of a charge localized at l is

$$Q(l,\tau)/Q_o = \exp[-\gamma'(l)\tau], \tag{4}$$

where $\gamma'(l) = A \exp(-l/l_o')$ and primes distinguish the electron return versus ejection direction. An important point here is that $l_o' = 1$ Å $(1\text{eV}/\Delta E')^{1/2}$ can in principle differ from l_o by virtue of different barrier heights for carrier ejection versus carrier return to the QD. For example, electron recovery can be to $E_{C\ \text{QD}}$ (or nonradiatively to $E_{V\ \text{QD}}$), whereas Auger assisted ionization can occur from higher energies (≈ 4.1–4.6 eV) and will often be inelastic, as shown in Fig. 3. This translates into a smaller (or larger) average barrier for QD charging vs neutralization, and provides a plausible mechanism for deviations in l_o'/l_o from unity.

The probability density for a trapping time of length τ is

$$P(l,\tau) = -\frac{dQ/d\tau}{Q} = \gamma'(l)\exp[-\gamma'(l)\tau], \tag{5}$$

from which the overall off-time probability distribution for an ensemble of switching events is

$$P(\tau_{\text{off}}) = \int f(l)P(l,\tau)dl$$
$$= \int \rho(l)\gamma(l)\gamma'(l)\exp[-\gamma'(l)\tau]dl/\rho_0 A l_0. \tag{6}$$

Here, for simplicity, the density of trap states is assumed constant to be consistent with the previous one-dimensional treatment of tunneling rates. Integrating Eq. (6) for constant $\rho(l)$ and taking the limit $(A\tau) \gg 1$ leads to

$$P(\tau)=\frac{(l_o'/l_o)A\Gamma(1+l_o'/l_o)}{(A\tau)^{1+l_o'/l_o}}, \tag{7}$$

where $\Gamma(1+l_o'/l_o)$ is the gamma function. Thus, the charging-tunneling model quite naturally yields a power law distribution in $P(\tau_{\rm off})$ for a single QD. Furthermore, the predicted power law exponent, $1+\alpha=1+l_o'/l_o$, can now differ from unity in a way that is physically motivated by the energetics in Fig. 3.

Of course, fundamental problems arise when this same model is applied to the $P(\tau_{\rm on})$ distribution; this is proportional to $dQ(\tau)/d\tau$ with $Q(\tau)$ given by Eq. (2a), which incorrectly yields an exponential decay. Furthermore, the time constant for this decay is short since τ_0 is given by the sum in Eq. (2b) and is dominated by the largest tunneling rates associated with the closest trap sites. Such a prediction contradicts two aspects of the experimental data; namely, that $P(\tau_{\rm on})$ is (i) well described by an inverse power law, and (ii) includes many long on times. It is worth stressing that this problem is fundamental to any static model where the on $\rightarrow$off rate is obtained by summing over multiple kinetic paths to many static trap sites.

It is tempting to fix this exponential $P(\tau_{\rm on})$ problem by proposing that the QD is initially turned off, by electron tunneling from a valence-band trap (Tr_+) impurity site to the QD (process No. 3, Fig. 3). The QD could then become fluorescent by electron transfer to an external conduction band trap site, (Tr_-), and switched back off when the ejected electron returns. The above $\tau^{-(1+\alpha)}$ dependence for electron return from Tr_- would then describe $P(\tau_{\rm on})$, whereas $P(\tau_{\rm off})$ now decays exponentially. Transferring this extra charge back and forth might then provide alternate intervals of inverse power-law $\tau_{\rm on}^{-(1+\alpha)}$ and $\tau_{\rm off}^{-(1+\alpha)}$ behaviors. However, several problems exist with this scenario. First, such a model would suggest negative charging of the QD, whereas positive charging is what is experimentally detected. Second, this model would incorrectly predict an exponential series of $\tau_{\rm on}$ (or $\tau_{\rm off}$) episodes with short average lifetimes, interspersed between a power law distribution of $\tau_{\rm off}$ (or $\tau_{\rm on}$) dominated by many long episodes, a scenario that is not observed. More fundamentally, this model implies multiple parallel paths to QD charging. If the second electron transfer event occurs independent of the first, then geminate recombination of the electron from the initially populated trap site is not necessary to switch the QD back on. With the fastest switching events dominating this kinetic sum over multiple parallel paths, inverse power-law behavior is subsequently lost. The existence of multiple parallel paths also makes the probability of long $\tau_{\rm on}$ and $\tau_{\rm off}$ episodes negligible, as described earlier.

This failure to predict power-law distributions in both $P(\tau_{\rm on})$ and $P(\tau_{\rm on})$ is explicitly linked to any scenario that involves a static environment of trap sites and tunneling barriers. In contrast, it is entirely possible that atom migration and bonding rearrangements open and close trap sites or vary barrier heights/widths. This is particularly likely in the presence of the $>$2-eV incident laser radiation, and is also consistent with observed spectral changes in the QD emission.[46] Other changes responsible for the on/off switching could arise from different bonding or atomic arrangements on the QD surface, including irreversible oxidation,[5,47] that produce nonradiative decay sites. However, regardless of origin, the number of such pathways available at any given time must be one (or a few at most) in order to prevent the summing/statistical averaging over multiple parallel rate processes that inevitably degrades the power law into simple exponential kinetic behavior.

This discussion leads to the following criteria for any physical model consistent with inverse power-laws in both $P(\tau_{\rm on})$ and $P(\tau_{\rm off})$. First, this behavior requires sampling an exponential distribution of QD decay rates for electron ejection/recombination [i.e., $\gamma(l)$ or $\gamma'(l)$], each time the QD switches on or off. Second, there can be only one pathway (or at most a few) for charging/recombination processes at any given time, in order to prevent a summing/statistical averaging over multiple routes and regression to exponential behavior. Finally, the lack of any correlation between successive on/off events requires the QD and environment to be dynamically fluctuating, with tunneling barriers changing randomly after each on/off event. Indeed, the absence of correlation between successive on/off events requires these changes in on/off rate constants to occur on the same timescale as the fluorescence intermittency, specifically *synchronized* with carrier ejection/recombination events.

D. Multiple surface charge model

At this point, a scenario that must be discussed is a ''multiple surface charge'' model. In this respect, it has been proposed that a number of charges decorate the surface of each QD.[46,48] The origin, type (electron or hole), number, and location of these multiple charges are not specified; however, such a situation could arise from the surface localization of one or both carriers upon photoexcitation of the QD. In this manner, the observation of single QD spectral diffusion (explained as originating from fluctuating local electric fields) as well as measurements of a large ground state dipole moment for either wurtzite or zinc-blende QDs in dielectric dispersion measurements can simultaneously be rationalized. Direct evidence of such surface localized charges can be seen in recent ensemble electron paramagnetic resonance and optically detected magnetic resonance experiments, where long-lived (10^{-6} sec to tens of minutes) signals associated with electrons and holes are observed, some light enhanced.[49,50] However, explaining on/off fluorescence intermittency within the context of such a multiple surface charge model is not necessarily obvious and in what follows we describe where such a model might succeed and where it appears to fail.

To start, a dynamic (fluctuating) tunnel barrier responsible for the on/off fluorescence intermittency can be recast, within the context of a multiple surface charge model, as the movement of QD surface charges that alters the effective (local) electric field experienced by the QD. In turn, such fluctuating electric fields and corresponding Coulomb potentials change both conduction band ($E_{c\ \rm QD}$, Fig. 3) and valence band energies ($E_{v\ \rm QD}$, Fig. 3), affecting the tunneling barrier height for carriers trying to leave (ionize) or return to

(neutralize) the QD. In this respect, we have previously shown that neither a static nor dynamic configuration of surface trap states can be solely responsible, for the long on-time/off-time intermittency. Rather, states *extrinsic* to the QD are needed to account for the 10^{-6}–10^{2} sec to minutes on/off times seen experimentally. To explain the lack of temperature dependence to the blinking kinetics, the movement of surface charges occurs, not as a consequence of thermally activated events (possibly due to ''deep'' surface traps), but rather through hopping/tunneling motion among available surface states. Consequently, an exponential distribution of QD on/off decay rates can explicitly be linked to an exponential tunneling probability (or waiting time distribution) of surface localized carriers between different trap sites, in turn causing a fluctuating tunneling barrier for carriers leaving the QD or returning to it from extrinsic trap sites. Note that we have implicitly assumed the *absence* of any communication between internal core carriers and external surface charges. As it turns out, this is an unrealistic assumption whose problems and consequences will be discussed in more detail below. Finally, the lack of correlation between subsequent on/off events can additionally be rationalized by the synchronized reorganization of surface charges, associated electric field, and effective tunneling barrier upon ionizing/neutralizing the QD.

One challenging problem with the above scenario arises from the efficient communication between internal core carriers and trapped surface charges. Simple calculations show that core carriers sample the surface frequently, leading one to speculate that internal carriers and trapped surface charges would undergo frequent electron-hole recombination (QD neutralization) events on sufficiently fast timescales to prevent long time on/off intermittency and power-law behavior. It takes only *one* of possibly *many* surface localized carriers to neutralize an ionized QD, turning it back on. To illustrate, given a 4-eV barrier, free-electron mass, and separations between 1 and 5 Å, resulting tunneling probabilities within a simple one-dimensional scenario are high, ranging from 10^{-1} to 10^{-5}. To sustain a 10-s off-time where one has a hole inside the QD and multiple electrons and/or holes decorating the surface of the QD, the internal hole must be immune to $>10^{12}$ possible recombination attempts with not just one nearby surface electron but many. Furthermore, the immunity possessed by the hole toward recombination or neutralization must occur not just once but many times during a given experiment, as witnessed by the abundance of long off times seen in experimental single QD fluorescence trajectories. For a multiple surface charge model to account for such long (μs to min) on/off times, internal/surface charge recombination events must therefore be exceedingly rare, and even more infrequent than tunneling events between a QD and an extrinsic trap site. The simultaneous presence of multiple surface charges and a requirement that they remain inaccessible to internal core carriers is therefore a paradox and represents the main conceptual difficulty in a multiple surface charge model. Indeed, in any model where independent motion of each carrier is invoked, the *fastest* charge transfer events between internal (core) and external (surface localized) charges will dominate any on/off intermittency kinetics, preventing long on-times and off-times as well as inverse power law behavior.

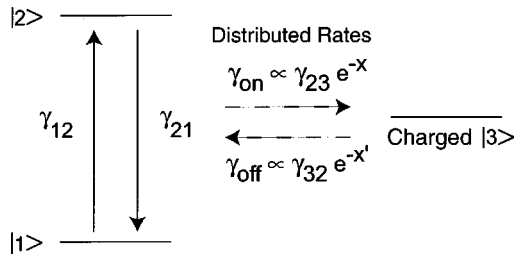

FIG. 4. Fluctuating barrier kinetic model. The ground state is denoted by $|1\rangle$ and the first excited state by $|2\rangle$. Ground-state/first-excited-state transitions are governed by the excitation rate γ_{12} and the QD radiative rate γ_{21}. Transitions to an ionized state, $|3\rangle$, are modeled by exponentially distributed γ_{on} and γ_{off} rates representing fluctuations in the QD and its local environment.

IV. PHENOMENOLOGICAL CHARGING-TUNNELING MODEL

A. Model description

Although further efforts will be required to unambiguously characterize the explicit chemical/physical pathway for QD blinking, we can nevertheless make progress by examining predictions of simple mathematical models for this phenomenon and, where appropriate, by making comparisons with experimental data. One such model, based on a three-level system with a QD ground state, $|1\rangle$, radiating (neutral) excited state, $|2\rangle$, and nonradiating (ionized) state, $|3\rangle$, is explicitly illustrated in Fig. 4. Transitions from $|1\rangle \rightarrow |2\rangle$ and $|2\rangle \rightarrow |1\rangle$ occur with rates γ_{12} and γ_{21}, respectively. Ionization and neutralization steps $|2\rangle \leftrightarrow |3\rangle$ occur with a range of rates that are exponentially distributed, switching randomly after each transition. The rates for leaving the ''on'' ($|2\rangle \rightarrow |3\rangle$) and ''off'' ($|3\rangle \rightarrow |2\rangle$) states, respectively, are expressed as

$$\gamma_{on}(x) = \gamma_{23} \exp(-x), \tag{8a}$$

$$\gamma_{off}(x') = \gamma_{32} \exp(-x'), \tag{8b}$$

where for an Auger-assisted ionization model the preexponential factor γ_{23} can, in general, depend on excitation intensity γ_{12}, and x and x' are stochastic variables. The normalized distributions of x, and x' are given by

$$L(x)_{on} = \alpha_{on} \exp(-\alpha_{on} x), \tag{8c}$$

$$L(x')_{off} = \alpha_{off} \exp(-\alpha_{off} x'), \tag{8d}$$

i.e., larger values of x, and x' are exponentially less likely to occur. One should note that the choice of carrier return from $|3\rangle$ to $|2\rangle$ instead of $|1\rangle$ implies no loss of generality, since any measurable ''on'' event requires many $|1\rangle \leftrightarrow |2\rangle$ cycles. In essence, this model is equivalent to applying the equations of the previous section, which only had significance to off $\rightarrow$on switching, to both on$\rightarrow$off and off$\rightarrow$on events.

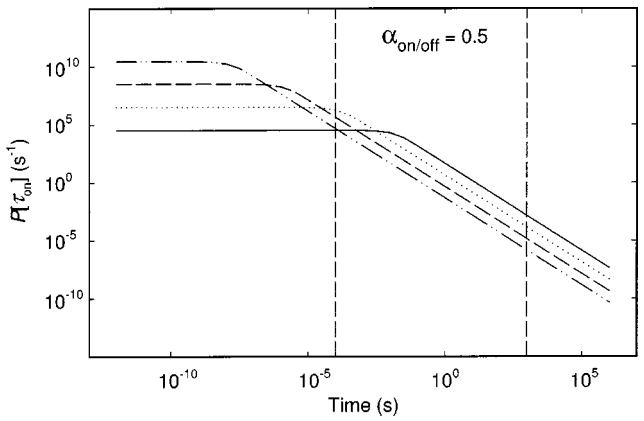

FIG. 5. Plot of Eq. (14) [or Eq. (11)] for $P(\tau_{on})$ $[P(\tau_{off})]$, when α_{on} $[\alpha_{off}]=0.5$. The prefactor γ_{23} $[\gamma_{32}]$ is varied from 10^9/s to 10^{12}/s (top to bottom, left side of graph). Regions between the dashed lines represent experimentally accessible time scales, coinciding with the $P(\tau_{on})$ $[P(\tau_{off})]$ power-law behavior.

We first consider the stochastic switching of a single QD. If the nanocrystal is initially ''off,'' with population only in $|3\rangle$, the rate of off→on transfer is given by

$$\frac{dn_3}{d\tau} = -\gamma_{32}e^{-x'}n_3, \tag{9}$$

where x' is selected from Eq. (8d). Integrating Eq. (9) yields $n_3(\tau)=\exp(-\gamma_{32}e^{-x'}\tau)$ and a probability density for switching ''on'' at time τ:

$$P(\tau,x')_{off} = -dn_3(\tau)/d\tau = \gamma_{32}e^{-x'}\exp(-\gamma_{32}e^{-x'}\tau). \tag{10}$$

Weighted by the probability $L(x')_{off}$, the average ensemble result is

$$P(\tau_{off}) = \int_0^\infty dx' L(x')_{off} P(\tau,x')_{off} = \frac{\alpha_{off}\Gamma(1+\alpha_{off},\gamma_{32}\tau)}{\tau^{1+\alpha_{off}}\gamma_{32}^{\alpha_{off}}}, \tag{11}$$

where Γ is the incomplete gamma function. For $\gamma_{32}\tau \ll 1$, $P(\tau_{off}) \cong \alpha_{off}(1+\alpha_{off})^{-1}\gamma_{32}$, whereas for $\gamma_{32}\tau \gg 1$, $P(\tau)_{off} \cong \alpha_{off}\gamma_{32}^{-\alpha_{off}}\Gamma(1+\alpha_{off})\tau^{-(1+\alpha_{off})}$. By way of example, $P(\tau_{off})$ from Eq. (11) is explicitly plotted versus τ in Fig. 5 for $\alpha_{off}=0.5$ and several values of γ_{32} varying from 10^9/s to 10^{12}/s. Note that the transition from time independent to power law behavior ($\gamma_{32}\tau \approx 1$) may or may not be within the window of experimentally accessible bin times, denoted by the region between the dashed lines in Fig. 5.

Similarly, if the population is initially ''on,'' (i.e., cycling between $|1\rangle$ and $|2\rangle$), then after an initial transient period $\sim 1/(\gamma_{21}+\gamma_{12})$, (n_1+n_2) decays exponentially to $|3\rangle$ as $\exp[-\gamma_{eff}(x)\tau]$, where

$$\gamma_{eff}(x) = \gamma_{12}\gamma_{23}e^{-x}/(\gamma_{12}+\gamma_{21}) = f\gamma_{on}(x), \tag{12a}$$

and

$$f = \gamma_{12}/(\gamma_{12}+\gamma_{21}) \tag{12b}$$

is the photoexcited fraction, $n_2/(n_1+n_2)$, in the upper state. Thus

$$P(\tau,x)_{on} = \gamma_{eff}(x)\exp[-\gamma_{eff}(x)\tau], \tag{13}$$

which when combined with $L(x)_{on}$ from Eq. 8(c) yields

$$P(\tau_{on}) = \int dx L(x)_{on} P(\tau,x)_{on} \cong \frac{\alpha_{on}\Gamma(1+\alpha_{on},\gamma_{23}\tau)}{\tau^{1+\alpha_{on}}\gamma_{23}^{\alpha_{on}}}. \tag{14}$$

The three-level model in Fig. 4, with randomly switched, exponentially weighted off→on and on→off rates, thus has sufficient flexibility to predict the observed on/off power-law distributions, as well as absence of correlation between successive on and off events.

B. Monte Carlo simulations

In an effort to compare more directly with experiment, Monte-Carlo simulations have been used to investigate the stochastic on/off blinking model discussed in the previous section. Emission is assumed to occur during $|2\rangle \rightarrow |1\rangle$ transitions, with these radiative events stored in bins. In the simulations, the excitation rate, γ_{12}, is varied between 5×10^5/s and 5×10^8/s, consistent with the absorption cross section and excitation intensities ($\sim$0.1–1 kW/cm^2) typically encountered in single-QD experiments.[5–13] The radiative rate γ_{21} is fixed at 1×10^7/s, i.e., consistent with the value obtained from these studies (vide infra). The choice of trapping/recovery rate prefactors, γ_{23} and γ_{32}, is motivated by experimental studies suggesting that relevant time scales for these prefactors may lie in a region between 10^5/s and 10^8/s.[12,14,51] Since more than 10^3 emitted photons are needed to unambiguously determine on vs. off, bin times (τ_{min}) are much larger than the characteristic times associated with γ_{12} and γ_{21}. Typically $\tau_{min}=1$ ms, with 0.5-ns time steps between computational evaluations. Exponential distributions of x and x' are obtained from $(1/\alpha_{on/off})\ln(1-y)$, with random selection of $0<y<1$. New x and x' values are randomly selected each time a transition is made from $|3\rangle \rightarrow |2\rangle$ or $|2\rangle \rightarrow |3\rangle$.

Figure 6 provides examples of such Monte Carlo simulations, holding $\gamma_{32}=1\times10^5$/s constant and independently varying γ_{12} and γ_{23}. Figures 6(a) and 6(b) correspond to a γ_{12} constant at 5×10^6/s, with γ_{23} varied from 5×10^6/s to 1×10^7/s. Figures 6(c) and 6(d) depict Monte Carlo simulations with $\gamma_{12}=1\times10^7$/s and γ_{23} varied from 1×10^7/s to 1×10^8/s. Note that since γ_{23} and γ_{32} determine the maximum ionization and return rate, the rate constant ratio $R \equiv \gamma_{23}/\gamma_{32}$, and more specifically the product of R times f, the fractional population in the upper state, controls the average on versus off character of the trajectory. For example, as the product fR increases from 2.5 to 500 in Figs. 6(a)–6(d), the trajectories experience more frequent off episodes. Note that the range of predicted fluorescence trajectories in Fig. 6 encompass the dynamic range of experimentally observed behaviors in Figs. 1 and 2, in terms of fractional ''on'' times, frequency, and duration of blinking events, etc.

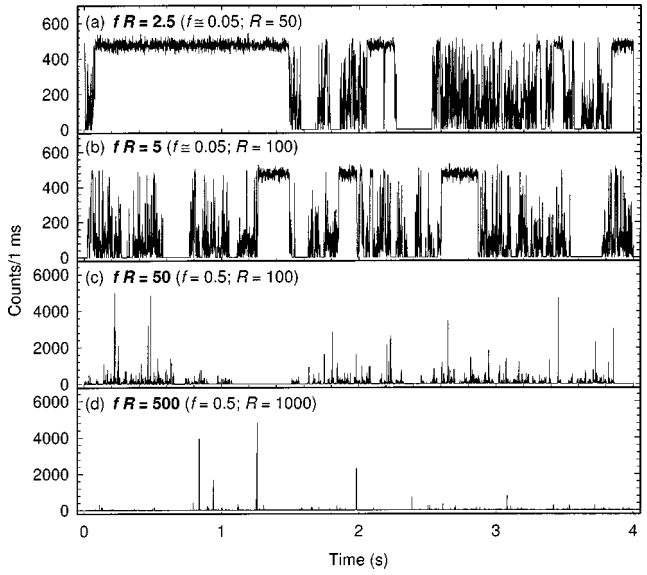

FIG. 6. Monte Carlo simulations, emphasizing the stochastic nature of the ''on''/''off'' fluorescence intermittency. In all cases, $\tau_{min}=1$ ms, $\gamma_{21}=10^7$/s, $\gamma_{32}=10^5$/s, and full trajectories span 80 s. Between (a) and (d), the product, fR, is varied from 2.5 to 500, showing corresponding changes in the on/off character of the trajectories. (a) $\gamma_{12}=5\times10^5$/s, $f=0.05$ and $R=50$. (b) $\gamma_{12}=5\times10^5$/s, $f=0.05$, and $R=100$. (c) $\gamma_{12}=10^7$/s, $f=0.5$, and $R=100$. (d) $\gamma_{12}=10^7$/s, $f=0.5$, and $R=1000$.

The Monte Carlo data are subsequently analyzed in the same manner as experimental fluorescence trajectories to obtain $P(\tau_{on/off})$. An intensity threshold is defined, with events above (below) it signaling ''on'' (''off'') transitions. Histograms of on and off times are constructed and their probability densities generated, employing the same algorithm used to analyze experimental trajectories.[11–13] Figures 7(a) and 7(b) show $P(\tau_{on})$ and $P(\tau_{off})$ from an analysis of Fig. 6(b), based on a threshold at 20% maximum intensity and an 80-s total trajectory. The power-law behavior in $P(\tau_{on/off})$ is clearly reproduced, with fitted power-law exponents $[m_{on}=2.21(7), m_{off}=1.96(4)]$ close to what is predicted $(1+\alpha_{on/off}\approx 2)$. Worth noting are the slight but systematic deviations from pure power law behavior in both $P(\tau_{on})$ and $P(\tau_{off})$ at short times, where the number of events are sufficiently large to expect good statistics. This is due to the finite bin size and choice of threshold, which undercount multiple on/off blinking events occurring during a single τ_{min}. This illustrates that additional information about blinking on faster time scales should be encoded within the intensity fluctuations and represents another potential avenue of investigation in the analysis of fluorescence intermittency,

C. Analysis: steady-state results and average values

The average result from a single QD that repeatedly cycles on-off should be equivalent to an average over an ensemble of QDs. Such ensembles can be modeled by employing transitions between $|2\rangle\rightarrow|3\rangle$ and $|3\rangle\rightarrow|2\rangle$ with average rates $\langle\gamma_{on}\rangle$ and $\langle\gamma_{off}\rangle$. Using $\langle\gamma_{on/off}\rangle$ in steady-state rate equations for the ensemble-average populations n_1, n_2, and n_3 yields

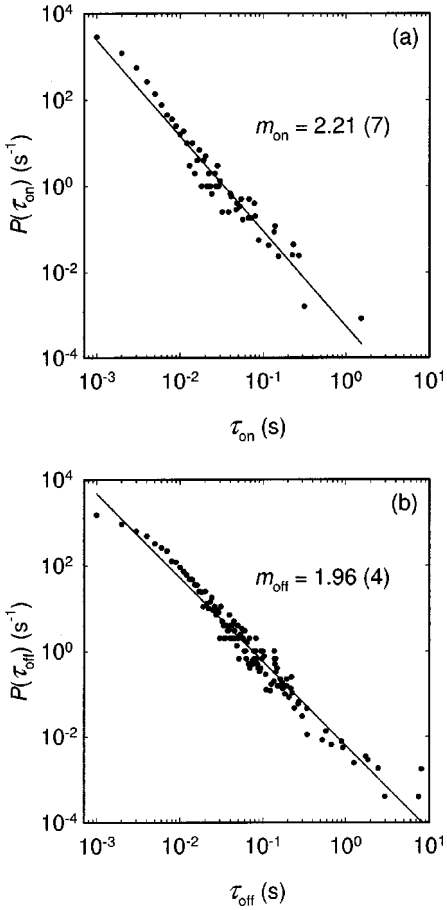

FIG. 7. Log-log plots of (a) $P(\tau_{on})$ and (b) $P(\tau_{off})$ generated from the Monte Carlo trajectory shown in Fig. 6(b). In all cases the threshold defining ''on'' from ''off'' is 100 counts/1 ms and the solid line is a linear fit to the data, suggesting a power-law behavior. Extracted slopes and standard errors are shown.

$$\frac{dn_1}{dt}=-\gamma_{12}n_1+\gamma_{21}n_2=0, \tag{15a}$$

$$\frac{dn_2}{dt}=\gamma_{12}n_1-(\gamma_{21}+\langle\gamma_{on}\rangle)n_2+\langle\gamma_{off}\rangle n_3=0, \tag{15b}$$

$$\frac{dn_3}{dt}=\langle\gamma_{on}\rangle n_2-\langle\gamma_{off}\rangle n_3=0. \tag{15c}$$

After a brief induction period$\gg(\gamma_{12}+\gamma_{21})^{-1}\approx 25$ ns, n_1 and n_2 achieve a steady state population ratio of $f=n_2/(n_1+n_2)=\gamma_{12}/(\gamma_{12}+\gamma_{21})$. If we neglect blinking, the fluorescence intensity is

$$I_{on}=f\gamma_{21}=\gamma_{12}\gamma_{21}/(\gamma_{12}+\gamma_{21}), \tag{16}$$

which is the maximum experimental intensity that can be observed for a given τ_{min}. If we include blinking, the average intensity per QD decreases to

$$\langle I_{\mathrm{Fl}}\rangle = n_2\gamma_{21} = \frac{\gamma_{12}\gamma_{21}}{\gamma_{21}+\gamma_{12}\left(1+\dfrac{\langle\gamma_{\mathrm{on}}\rangle}{\langle\gamma_{\mathrm{off}}\rangle}\right)}$$

$$= \frac{\gamma_{21}}{\left(1+\gamma_{21}/\gamma_{12}+\dfrac{\langle\gamma_{\mathrm{on}}\rangle}{\langle\gamma_{\mathrm{off}}\rangle}\right)}. \tag{17}$$

The average fraction of time a single QD is in the on state (i.e., in *either* state 1 or 2) can now be defined as

$$\langle F_{\mathrm{on}}\rangle = \left(1+f\frac{\langle\gamma_{\mathrm{on}}\rangle}{\langle\gamma_{\mathrm{off}}\rangle}\right)^{-1}. \tag{18}$$

Equations (16)–(18) constitute the three experimental observables that we wish to predict from the model parameters. For a sum over sequential single particle events, the average steady state rate is given by

$$\langle\gamma_{\mathrm{on/off}}\rangle = 1/\langle\tau_{\mathrm{on/off}}\rangle, \tag{19}$$

where $\langle\tau_{\mathrm{on/off}}\rangle$ is the average time spent in and $\langle\gamma_{\mathrm{on/off}}\rangle$ is the average rate for decaying out of the on or off state. $\langle\tau_{\mathrm{on/off}}\rangle$ can be obtained from the known power-law distribution

$$\langle\tau_{\mathrm{on/off}}\rangle = \int_0^{\{\tau_{\mathrm{on/off}}\}_{\max}} d\tau P(\tau_{\mathrm{on/off}})\tau, \tag{20}$$

with $P(\tau_{\mathrm{on/off}})$ given by Eqs. (11) and (14) and $\{\tau_{\mathrm{on/off}}\}_{\max}$ obtained from the maximum $\tau_{\mathrm{on/off}}$ observed in a given data set. However, since the average time for a single "on" $\leftrightarrow$ "off" event is $\tau_{\mathrm{on/off}}(x)=1/\gamma_{\mathrm{on/off}}(x)=1/(\gamma_{23/32}e^{-x})$, $\langle\tau_{\mathrm{on/off}}\rangle$ can be evaluated most directly as the average of $\tau_{\mathrm{on/off}}(x)$ weighted by $L(x)_{\mathrm{on/off}}$,

$$\langle\tau_{\mathrm{on/off}}\rangle = \int_0^{X_{\mathrm{on/off}}} dx L(x)_{\mathrm{on/off}}\tau(x)_{\mathrm{on/off}}, \tag{21}$$

where $X_{\mathrm{on/off}}$ is the maximum value of x corresponding to the $\{\tau_{\mathrm{on/off}}\}$ upper limit in Eq. (20). For present purposes, it suffices to require that $L(X_{\mathrm{on/off}})\times N\approx 1$, or equivalently that $\{\tau_{\mathrm{on/off}}\}_{\max}=1/\gamma_{\mathrm{on/off}}(\alpha_{\mathrm{on/off}}N)^{1/\alpha_{\mathrm{on/off}}}$ where N is the maximum number of observed on/off switching events. Thus in the same limit of $(\gamma\tau)\gg 1$, one finds $(0<\alpha_{\mathrm{on/off}}<1)$

$$\langle\tau\rangle = \frac{\alpha^{1/\alpha}}{1-\alpha}N^{(1-\alpha)/\alpha}\gamma^{-1} \tag{22}$$

for both "on" and "off" subscripts. Repeated application also yields

$$\frac{\langle\gamma_{\mathrm{on}}\rangle}{\langle\gamma_{\mathrm{off}}\rangle} = \frac{\langle\tau_{\mathrm{off}}\rangle}{\langle\tau_{\mathrm{on}}\rangle} = \frac{\alpha_{\mathrm{off}}^{1/\alpha_{\mathrm{off}}}}{\alpha_{\mathrm{on}}^{1/\alpha_{\mathrm{on}}}}\left(\frac{1-\alpha_{\mathrm{on}}}{1-\alpha_{\mathrm{off}}}\right)N^{(1/\alpha_{\mathrm{off}})-(1/\alpha_{\mathrm{on}})}\left(\frac{\gamma_{\mathrm{on}}}{\gamma_{\mathrm{off}}}\right), \tag{23}$$

which for a given N can be used to estimate the experimental observables in Eqs. (17) and (18).

In order to test these predictions against Monte Carlo results, average fluorescence intensities, $\langle I_{\mathrm{Fl}}\rangle/\gamma_{21}$, are plotted in Figs. 8(a) and 8(b) versus the excitation rate ratio γ_{12}/γ_{21} for a series of $R=\gamma_{23}/\gamma_{32}$ values. Since $\gamma_{12}=I_L\sigma/h\nu$, this is essentially equivalent to plotting the fractional population in $|2\rangle$ against excitation intensity I_L. In Fig. 8(a), we first take γ_{23} to be independent of I_L. Within this "direct tunneling" model, $\langle I_{\mathrm{Fl}}\rangle/\gamma_{21}$ rises linearly with laser intensity and then saturates at $1/(1+R)$, where $R=\gamma_{23}/\gamma_{32}$. Good agreement is obtained with the corresponding $\langle I_{\mathrm{Fl}}\rangle/\gamma_{21}$ values from the Monte Carlo simulations (open circles), for γ_{23} and γ_{32} preexponential factors corresponding to $R\approx 10-100$. Dark circles indicate the corresponding maximum fluorescence rates, $\langle I_{\mathrm{Fl}}\rangle_{\max}=I_{\mathrm{on}}$, again in excellent agreement with the steady state results of Eq. (16). To help assess the validity of

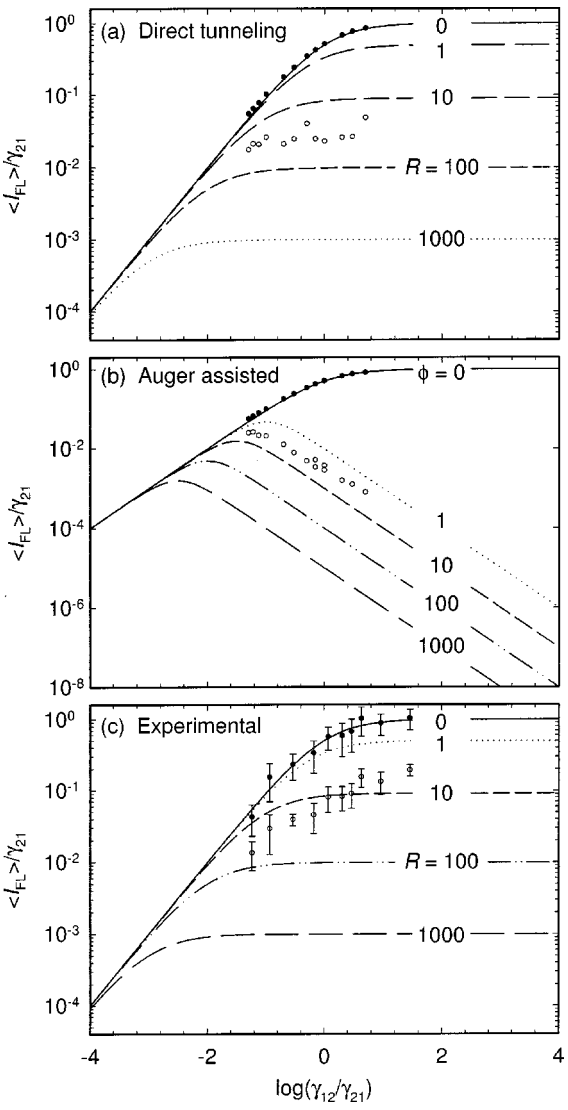

FIG. 8. Plot of the average fluorescence intensity, $\langle I_{\mathrm{FL}}\rangle/\gamma_{21}$, vs the excitation rate ratio γ_{12}/γ_{21} [Eq. (17) in the text]. (a) Direct tunneling model, where γ_{23} is independent of I_L and where different lines represent variations in $R=\gamma_{23}/\gamma_{32}$. (b) Auger-assisted tunneling model where $\gamma_{23}=\phi\gamma_{12}$. Different lines represent variations in ϕ. In both (a) and (b) the closed (open) symbols are maximum (average) data taken from an analysis of Monte Carlo trajectories. (c) Comparison to experiment where the closed (open) symbols are maximum (average) normalized intensities taken from an analysis of experimental data. Lines represent predictions for a direct tunneling model.

an alternative ''Auger-assisted'' mechanism for QD ionization, we have also performed Monte Carlo calculations for a multiple photon model, where the ionization rate γ_{23}, increases linearly with laser intensity. Analytic predictions of this $\gamma_{23}=\phi\gamma_{12}$ model are plotted in Fig. 8(b) for several values of ϕ, and they are compared with the Monte Carlo results. Note that for any finite ionization rate (i.e., $\phi\neq 0$), the average fluorescence rate first increases but eventually decreases with I_L, due to more efficient two-photon ionization of the QD. This is in good agreement with the results from Monte Carlo simulations of $\langle I_{\mathrm{Fl}}\rangle/\gamma_{21}$ for $\phi\approx 1$ (open circles) and maximum fluorescence rates $\langle I_{\mathrm{Fl}}\rangle_{\max}/\gamma_{21}$ when $\phi\approx 0$ (closed circles). However, these ''Auger-assisted'' tunneling predictions prove to be in poor agreement with experimental data [Fig. 8(c)], as will be discussed in more detail in Sec. V.

Next we turn to $\langle F_{\mathrm{on}}\rangle$, the fractional time spent in the on state. The results from Monte Carlo simulations are plotted in Figs. 9(a) and 9(b) vs the excitation rate ratio $(\gamma_{12}/\gamma_{21})$ for a series of (a) R and (b) ϕ values for the ''direct'' and ''Auger assisted'' tunneling models, respectively. For the ''direct'' tunneling model, $\langle F_{\mathrm{on}}\rangle$ falls from unity at low excitation intensity down to an asymptotic limit of $1/R$ at high intensity. By way of contrast, the Auger-assisted model predicts no such saturation effect, continuing to decrease uniformly with higher excitation rates due to the increasingly efficient two-photon ionization of the QD. Monte Carlo results for the direct tunneling model are presented in Fig. 9(a) (closed circles) for $\alpha_{\mathrm{on}}=\alpha_{\mathrm{off}}=1$ and indicate good agreement with the corresponding $R=\gamma_{23}/\gamma_{32}\approx 100$ curve. Similarly, Monte Carlo data for the ''Auger-assisted'' tunneling mechanism are shown in Fig. 9(b) (dark circles), and are consistent with corresponding model predictions from Eq. (18) for $\phi=10$. However, such Auger model predictions of a uniform decrease in $\langle F_{\mathrm{on}}\rangle$ with increasing excitation intensity appear unsupported by experimental measurements previewed in Fig. 9(c). Though details of this analysis are deferred to the next section, the data in Fig. 9(c) show a more nearly saturated dependence of $\langle F_{\mathrm{on}}\rangle$ with increasing laser excitation, once again in better agreement with predictions from a direct tunneling vs ''Auger-assisted'' tunneling model.

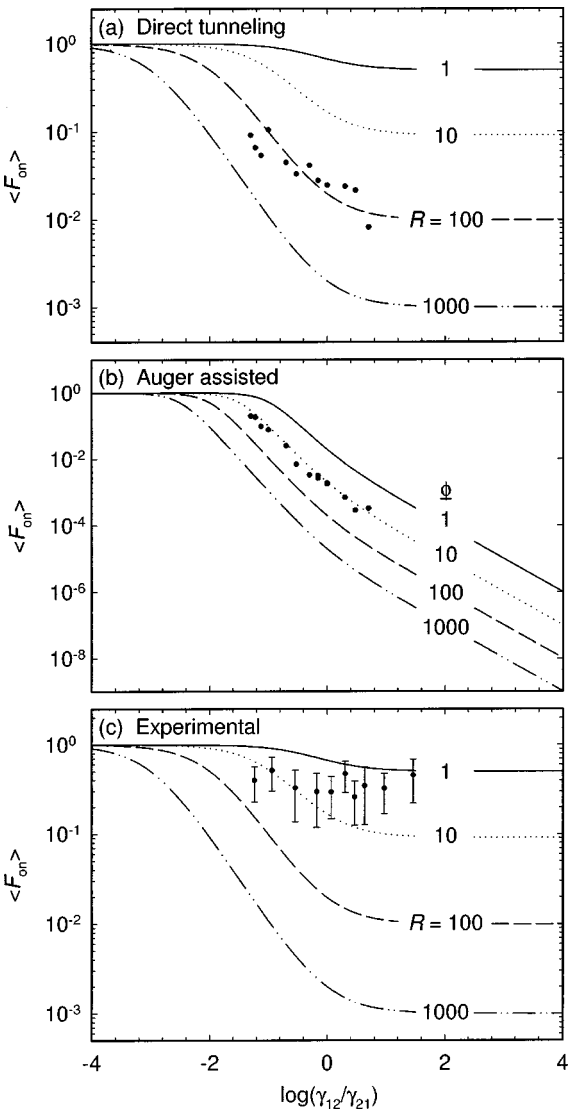

FIG. 9. Plot of the average fractional on time, $\langle F_{\mathrm{on}}\rangle$, vs the excitation rate ratio γ_{12}/γ_{21} [Eq. (18) in the text]. (a) Direct tunneling model where γ_{23} is independent of I_L. Lines represent different $R=\gamma_{23}/\gamma_{32}$ ratios. (b) Auger-assisted tunneling model where $\gamma_{23}=\phi\gamma_{12}$. Different lines represent variations in ϕ. In both (a) and (b) closed symbols represent data extracted from an analysis of Monte Carlo data. (c) Comparison to experiment where the closed symbols represent data taken from an analysis of experimental trajectories. Lines are predictions of a direct tunneling model.

V. DISCUSSION AND COMPARISON WITH EXPERIMENT

The mathematical analysis presented in Sec. IV C identifies several key observables that can be used to critically evaluate the models presented herein. The three most accessible experimental quantities are (i) I_{on}, the maximum fluorescence intensity; (ii) $\langle I_{\mathrm{Fl}}\rangle$, the average fluorescence intensity, and (iii) $\langle F_{\mathrm{on}}\rangle$, the fractional on time. We consider these in turn.

The maximum fluorescence intensity, given by Eq. (16), is simply the photostationery fractional population (f) in n_2 times the intrinsic radiative rate (γ_{21}). This fluorescence intensity can be related to the maximum experimentally observed fluorescence count rates by $I_{\max}=\beta I_{\mathrm{on}}$, where β is the photon collection efficiency of the confocal microscope and I_{on} is the actual maximum emission rate of the QD. Inserting this into Eq. (16), one obtains

$$\beta/I_{\max}=1/\gamma_{12}+1/\gamma_{21}. \tag{24}$$

The excitation rate can be obtained from the measured laser intensity at the focus of the microscope, which is converted to γ_{12} using the measured QD absorption cross section[12] at 488 nm, $\sigma_{488}\sim 4\times 10^{-15}$ cm^2. Equation (24) therefore predicts a linear relationship between $1/I_{\max}$ and $1/\gamma_{12}$, with a slope $1/\beta$ and an intercept corresponding to the radiative lifetime $\tau_{21}=1/\gamma_{21}$. The data presented in Fig. 10 clearly support the expected linear trend and can be subject to a

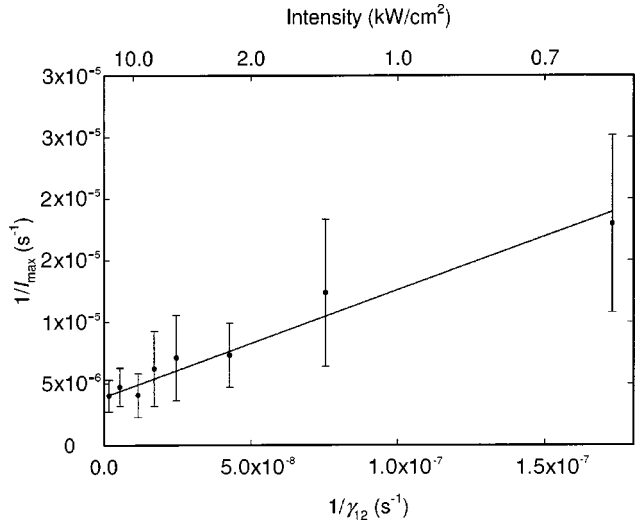

FIG. 10. Plot of the inverse maximum emission rate ($1/I_{max}$) from 27-Å radius CdSe QDs vs inverse the excitation rate ($1/\gamma_{12}$), assuming $\sigma_{488}\sim 4\times 10^{-15}$ cm^2 [Eq. (24) in the text]. The line is a weighted least squares fit to the data, yielding an effective collection efficiency of $\beta=1.2(1)\%$ and a radiative rate of $\gamma_{21}\approx 2\times 10^7$/s ($\tau_{rad}\approx 50$ ns).

weighted least squares analysis. The fitted slope yields $\beta=1.2(1)\%$, which is consistent with the reported microscope collection efficiency[12] of 0.87 (1)%. Of more fundamental interest is the QD radiative rate, which from β and the fitted intercept is $\gamma_{21}\cong 2\times 10^7$/s or $\tau_{rad}\cong 50$ ns. This value is comparable to recent ensemble and single QD lifetime measurements, indicating τ_{rad} to be between 20 and 30 ns.[14,51–54]

Calibration of photon collection efficiency and radiative lifetime permits us to extend this analysis one step further. Specifically, the average fluorescence rate, $\langle I_{Fl}\rangle$, expressed in Eq. (17) can now be evaluated from the averages measured experimentally. Additionally, this average fluorescence rate can be scaled by the experimentally measured γ_{21} to yield the (unitless) fractional population in the upper radiating state, i.e., $\langle n_2\rangle$. Of special relevance, this can now be compared with Monte Carlo predictions for both the ''direct'' and ''Auger-assisted'' tunneling models. The quantitative comparison for maximum fluorescence (I_{on}/γ_{21}; solid circles) and average fluorescence ($\langle I_{Fl}/\gamma_{21}\rangle$, open circles) intensities is demonstrated in Fig. 8(c). As expected from Eq. (16), the experimental I_{on}/γ_{21} data show a clear saturation of the maximum emission rate at high excitation rates. There is also quite good agreement with the intensity onset where saturation occurs, which is sensitive to the appropriate choice of γ_{12}/γ_{21}. Most interesting, though, is the behavior of $\langle I_{Fl}/\gamma_{21}\rangle$ (open symbols), which also shows clear evidence of saturation at high excitation rates. This is in excellent agreement with Eq. (17) and suggests an on→off and off→on rate constant ratio of $R=\gamma_{23}/\gamma_{32}\sim 10$. Furthermore, this is clearly inconsistent with any nonlinear two-photon mechanism for electron ejection. By way of example, for ''Auger-assisted'' tunneling where γ_{23} varies linearly with γ_{12}, the Monte Carlo simulations in Fig. 8(b) predict the average emission rate to drop by nearly two orders of magnitude over the range of excitation intensities investigated.

As a final note of comparison, experimental $\langle F_{on}\rangle$ values are plotted against excitation intensity in Fig. 9(c). There does not appear to be any significant change in the average fractional on time over the γ_{12}/γ_{21} range studied, though more subtle trends may be obscured by statistical uncertainties in the measurements. This is only marginally consistent with the $\gamma_{23}/\gamma_{32}\sim 10$ predictions from Eq. (18), but is clearly in qualitative disagreement with the Auger-assisted tunneling predictions (i.e., $\gamma_{23}\propto\gamma_{12}$) depicted in Fig. 9(b).

VI. SUMMARY AND CONCLUSION

The experimental comparisons in Figs. 8–10, as well as the corresponding Monte Carlo simulations, suggest that the proposed phenomenological QD switching model accounts for much of the fluorescence blinking behavior observed in isolated semiconductor QDs. Monte Carlo simulations of the model agree well with experimental on/off fluorescence trajectories and explain their intensity-dependent behavior. Specifically, at low excitation rates there are long periods of fluorescence with a relatively well-defined single ''on'' intensity. At high intensities, however, where $fR\gg 1$, both model and data reveal that on episodes are typically brief and the fluorescence intensity fluctuates severely.

Analytic solutions to the model, based on exponentially distributed tunneling rates for turning the QD on or off, begin to elucidate why inverse power laws are seen in *both* $P(\tau_{on})$ and $P(\tau_{off})$. This is because tunneling rates vary exponentially with both distance and barrier height, thus permitting a small dynamic range in either parameter to translate into large on↔off rate variations. Furthermore, the model successfully corroborates the behavior of $\langle I_{on}/\gamma_{21}\rangle$, $\langle I_{Fl}/\gamma_{21}\rangle$, and $\langle F_{on}\rangle$ in both experimental and Monte Carlo data. Specifically, the much improved agreement between experiment and predictions of a direct tunneling model are in strong support of conduction band carrier tunneling rather than Auger-assisted tunneling as the dominant mechanism for QD charging and blinking kinetics.

If tunneling-induced QD charging and reneutralization are responsible for the fluorescence intermittency, the identity of the states to which the carrier tunnels is of crucial importance. Based on physical barrier heights and characteristic times for the longest and shortest on/off events, states 1–2 nm away from the QD are likely to be responsible. Fused silica surface defects or impurity states may therefore be involved, suggesting that altering the substrate or increasing its cleanliness and/or homogeneity could have a major impact in better understanding and/or controlling fluorescence intermittency. These conclusions may also have broader implications for other systems, since the simple assertion that a single fluorophore interacts strongly with the local environment (through tunneling or otherwise) is likely to be a common feature underlying single molecule photophysics.

ACKNOWLEDGMENTS

Financial support for this work was provided by the National Institute of Standards and Technology and the National Science Foundation. We thank F. V. Mikulec and M. G. Bawendi for providing samples of CdSe QDs. M. K. thanks the National Research Council for a postdoctoral fellowship during part of this work.

*Present address: Stanford University, Department of Chemistry and Biochemistry.

†Staff Member, Quantum Physics Division, NIST.

‡To whom correspondence should be addressed. Electronic mail: Djn@colorado.edu

[1] W. P. Ambrose and W. E. Moerner, Nature (London) **349**, 225 (1991).

[2] Th. Basche, W. E. Moerner, M. Oritt, and H. Talon, Phys. Rev. Lett. **69**, 1516 (1992).

[3] A. C. J. Brouwer, E. J. J. Groenen, and J. Schmidt, Phys. Rev. Lett. **80**, 3944 (1998).

[4] J. A. Veerman, M. F. Garcia-Parajo, L. Kuipers, and N. F. van Hulst, Phys. Rev. Lett. **83**, 2155 (1999).

[5] M. Nirmal, B. O. Dabbousi, M. G. Bawendi, J. J. Macklin, J. K. Trautman, T. D. Harris, and L. E. Brus, Nature (London) **383**, 802 (1996).

[6] J. Tittel, W. Gohde, F. Koberling, A. Mews, A. Kornowski, H. Weller, A. Eychmuller, and Th. Basche, Ber. Bunsenges. Phys. Chem. **101**, 1626 (1997).

[7] F. Koberling, A. Mews, and Th. Basche, Adv. Mater. **13**, 672 (2001).

[8] U. Banin, M. Bruchez, A. P. Alivisatos, T. Ha, S. Weiss, and D. S. Chemla, J. Chem. Phys. **110**, 1195 (1999).

[9] K. T. Shimizu, R. G. Neuhauser, C. A. Leatherdale, S. A. Empedocles, W. J. Woo, and M. G. Bawendi, Phys. Rev. B **63**, 5316 (2001).

[10] W. G. J. H. M. van Sark, P. L. T. M. Frederix, D. J. van den Heuvel, M. A. H. Asselbergs, I. Senf, and H. C. Gerritsen, Single Mol. **1**, 291 (2000).

[11] M. Kuno, D. P. Fromm, H. F. Hamann, A. Gallagher, and D. J. Nesbitt, J. Chem. Phys. **112**, 3117 (2000).

[12] M. Kuno, D. P. Fromm, H. F. Hamann, A. Gallagher, and D. J. Nesbitt, J. Chem. Phys. **115**, 1028 (2001).

[13] M. Kuno, D. P. Fromm, A. Gallagher, D. J. Nesbitt, O. I. Micic, and A. J. Nozik, Nano Lett. **1**, 557 (2001).

[14] G. Messin, J. P. Hermier, E. Giacobino, P. Desbiolles, and M. Dahan, Opt. Lett. **26**, 1891 (2001).

[15] M. E. Pistol, P. Castrillo, D. Hessman, J. A. Prieto, and L. Samuelson, Phys. Rev. B **59**, 10 725 (1999).

[16] M. D. Mason, G. M. Credo, K. D. Weston, and S. K. Buratto, Phys. Rev. Lett. **80**, 5405 (1998); M. D. Mason, D. J. Sirbuly, P. J. Carson, and S. K. Buratto, J. Chem. Phys. **114**, 8119 (2001).

[17] M. A. Bopp, Y. Jia, L. Li, R. Cogdell, and R. M. Hochstrasser, Proc. Natl. Acad. Sci. USA **94**, 10 630 (1997).

[18] R. M. Dickson, A. B. Cubitt, R. Y. Tsien, and W. E. Moerner, Nature (London) **388**, 355 (1997).

[19] E. J. G. Peterman, S. Brasselet, and W. E. Moerner, J. Phys. Chem. A **103**, 10 553 (1999).

[20] P. Schwille, S. Kummer, A. A. Heikal, W. E. Moerner, and W. W. Webb, Proc. Natl. Acad. Sci. USA **97**, 151 (2000).

[21] D. Vanden Bout, W. T. Yip, D. Hu, D. K. Fu, T. M. Swager, and P. F. Barbara, Science **277**, 1074 (1997).

[22] R. Rodrigues-Herzog, F. Trotta, H. Bill, J. M. Segura, B. Hecht, and H. J. Guntherodt, Phys. Rev. B **62**, 11 163 (2000).

[23] M. D. Barnes, A. Mehta, T. Thundat, R. N. Bhargava, V. Chabra, and B. Kulkarni, J. Phys. Chem. B **104**, 6099 (2000).

[24] H. P. Lu and X. S. Xie, Nature (London) **385**, 143 (1997).

[25] T. Ha, Th. Enderle, D. S. Chemla, P. R. Selvin, and S. Weiss, Chem. Phys. Lett. **271**, 1 (1997).

[26] K. D. Weston, P. J. Carson, H. Metiu, and S. K. Buratto, J. Chem. Phys. **109**, 7474 (1998).

[27] R. J. Cook and H. J. Kimble, Phys. Rev. Lett. **54**, 1023 (1985).

[28] W. Nagourney, J. Sandberg, and H. Dehmelt, Phys. Rev. Lett. **56**, 2797 (1986); J. C. Bergquist, R. G. Hulet, W. M. Itano, and D. J. Wineland, *ibid.* **57**, 1699 (1986); Th. Sauter, W. Neuhauser, R. Blatt, and P. E. Toschek, *ibid.* **57**, 1696 (1986).

[29] Th. Basche, S. Kummer, and C. Brauchle, Nature (London) **373**, 132 (1995).

[30] X. S. Xie and R. C. Dunn, Science **266**, 1018 (1994).

[31] H. P. Lu and X. S. Xie, Nature (London) **385**, 143 (1997).

[32] T. Ha, Th. Enderle, D. S. Chemla, P. R. Selvin, and S. Weiss, Chem. Phys. Lett. **271**, 1 (1997).

[33] W. T. Yip, D. Hu, J. Yu, D. A. Vanden Bout, and P. F. Barbara, J. Phys. Chem. A **102**, 7564 (1998).

[34] C. Eggeling, J. Widengren, R. Rigler, and C. A. M. Seidel, in *Applied Fluorescence in Chemistry, Biology and Medicine*, edited by W. Rettig, B. Strehmel, S. Schrader, and H. Seifert, (Springer, Berlin, 1999) p. 193.

[35] M. P. Bruchez, M. Moronne, P. Gin, S. Weiss, and A. P. Alivisatos, Science **281**, 2013 (1998); W. C. Chan and S. Nie, *ibid.* **281**, 2016 (1998).

[36] X. G. Peng, M. C. Schlamp, A. V. Kadavanich, and A. P. Alivisatos, J. Am. Chem. Soc. **119**, 7019 (1997).

[37] B. O. Dabbousi, J. R. Viejo, F. V. Mikulec, J. R. Heine, H. Mattoussi, R. Ober, K. F. Jensen, and M. G. Bawendi, J. Phys. Chem. B **101**, 9463 (1997).

[38] M. A. Hines and P. Guyot-Sionnest, J. Phys. Chem. **468**, 100 (1996).

[39] C. B. Murray, D. J. Norris, and M. G. Bawendi, J. Am. Chem. Soc. **115**, 8706 (1993).

[40] M. Kuno, J. K. Lee, B. O. Dabbousi, F. V. Mikulec, and M. G. Bawendi, J. Chem. Phys. **106**, 9869 (1997).

[41] Al. L. Efros and M. Rosen, Phys. Rev. Lett. **78**, 1110 (1997).

[42] T. D. Krauss and L. E. Brus, Phys. Rev. Lett. **83**, 4840 (1999).

[43] A. J. Moses, *Optical Materials Properties* (IFI/Plenum, New York, 1971); J. C. Wurst, University of Dayton, Dayton, Ohio, Quarterly Progress Report No. 1, UDR1-QPR-71-10, Contract F33615-72-C-R57, Wright Patterson Air Force Base, Ohio; *CRC Handbook of Chemistry and Physics*, edited by D. R. Lide (CRC Press, Boca Raton, FL, 1990).

[44] S. A. Blanton, M. A. Hines, and P. Guyot-Sionnest, Appl. Phys. Lett. **69**, 3905 (1996).

[45] J. T. Randall and M. H. F. Wilkins, Proc. R. Soc. London, Ser. A **184**, 366 (1945).

[46] S. A. Empedocles and M. G. Bawendi, Science **278**, 2114 (1997).

[47] W. G. J. H. M. van Sark, P. L. T. M. Frederix, D. J. Van den

Heuvel, H. C. Gerritsen, A. A. Bol, J. N. J. van Lingen, C. de Mello Donega, and A. Meijerink, J. Phys. Chem. B **105**, 8281 (2001).

[48] M. Shim and P. Guyot-Sionnest, J. Chem. Phys. **11**, 6955 (1999); S. A. Empedocles and M. G. Bawendi, J. Phys. Chem. B **103**, 1826 (1999); L-W. Wang, *ibid.* **105**, 2360 (2001).

[49] O. I. Micic, A. J. Nozik, E. Lifshitz, T. Rajh, O. G. Poluektov, M. C. Thurnauer, J. Phys. Chem. B **106**, 4390 (2002); L. Langof, E. Ehrenfreund, E. Lifshitz, O. I. Micic, and A. J. Nozik, *ibid.* **106**, 1606 (2002); E. Lifshitz, A. Glozman, I. D. Litvin, and H. Porteanu, *ibid.* **104**, 10 449 (2000).

[50] M. Kuno, Ph.D. thesis, MIT, 1998.

[51] P. Michler, A. Imamoglu, M. D. Mason, P. J. Carson, G. F. Strouse, and S. K. Burratto, Nature (London) **406**, 968 (2000).

[52] B. Lounis, H. A. Bechtel, D. Gerion, P. Alivisatos, and W. E. Moerner, Chem. Phys. Lett. **329**, 399 (2000).

[53] M. Dahan, T. Laurence, F. Pinaud, D. S. Chemla, A. P. Alivisatos, M. Sauer, and S. Weiss, Opt. Lett. **26**, 825 (2001).

[54] G. Schlegel, J. Bohnenberger, I. Potapova, and A. Mews, Phys. Rev. Lett. **88**, 137401 (2002).